

Neural Architecture Search for Compressed Sensing Magnetic Resonance Image Reconstruction

Jiangpeng Yan, Shuo Chen, Xiu Li, *Member, IEEE*, and Yongbing Zhang, *Member, IEEE*

Abstract—Recent works have demonstrated that deep learning (DL) based compressed sensing (CS) implementation can provide impressive improvements to reconstruct high-quality MR images from sub-sampling k-space data. However, network architectures adopted in current methods are all designed by handcraft, thus the performances of these networks are limited by researchers' expertise and labor. In this manuscript, we proposed a novel and efficient MR image reconstruction framework by Neural Architecture Search (NAS) algorithm. The inner cells in our reconstruction network are automatically defined from a flexible search space in a differentiable manner. Comparing to previous works where only several common convolutional operations are tried by human, our method can explore different operations (e.g. dilated convolution) with their possible combinations sufficiently. Our proposed method can also reach a better trade-off between computation cost and reconstruction performance for practical clinical translation. Experiments performed on a publicly available dataset show that our network produces better reconstruction results compared to the previous state-of-the-art methods in terms of PSNR and SSIM with 4 times fewer computation resources. The final network architecture found by the algorithm can also offer insights for network architecture designed in other medical image analysis applications.

Index Terms—Compressed Sensing, Deep Learning, Magnetic Resonance Imaging, Neural Architecture Search.

I. INTRODUCTION

MAGNETIC Resonance Imaging (MRI) is a popular medical imaging modality which can offer high resolution and various contrast underlying anatomy images with low radiation and no invasion. However, the original data of MR images are acquired by sequentially scanning in k-space (i.e. Fourier space), and the speed of scanning is limited by physiological and hardware constraints [1]. The significant

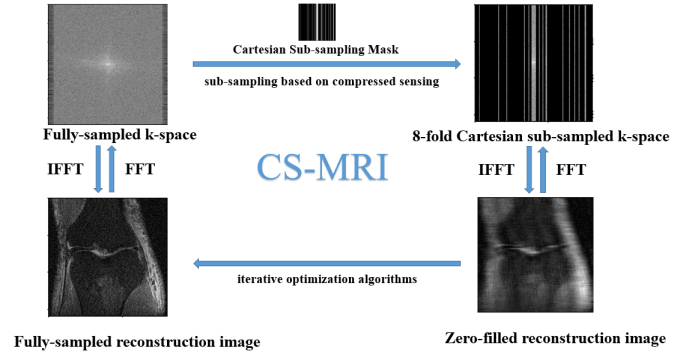


Fig. 1. An illustration of traditional CS-MRI acceleration framework. First, CS-MRI accelerates the k-space signals acquisition process by sub-sampling. Then, zero-filled reconstruction images are achieved by performing Inverse Fast Fourier Transform (IFFT) on sub-sampled k-space data. Finally, high quality MR images can be reconstructed by alleviating aliasing patterns in the zero-filled reconstruction images using iterative optimization algorithms. In this case, an 8-fold Cartesian sub-sampled mask is applied in k-space data, thus the signals acquisition process can be accelerated 8 times theoretically.

slow signal acquisition process makes MRI motion sensitive and less accessible for patients. Thus, MRI acceleration has been an active research area since it is proposed in the 1970s [2].

Among MRI acceleration methods, Compressed Sensing Magnetic Resonance Imaging (CS-MRI) gains much attention because this method does not need any additional hardware [3]. The key principle of compressed sensing [4] is that we can reconstruct images from sub-Nyquist sampling signals when the following two assumptions are satisfied: first, the images have a sparse representation in a specific transform domain; second, the sampling and the sparsity domain are incoherent. Based on compressed sensing theory, we can reconstruct MR images from random sub-sampled k-space data by using iterative optimization algorithms to suppress the aliasing patterns, i. e. incoherent noise, caused by the missing signals. Thus, the major problem of CS-MRI transfers to: 1) designing better sparse representation for de-aliasing; 2) efficient implementation for clinical translation. The whole framework of CS-MRI is shown in Fig. 1.

Recently, Deep Learning (DL) [5] has achieved a dominating position in many computer vision applications including object detection [6], semantic segmentation [7], image denoising [8], image super-resolution [9], etc. Consequently,

Manuscript received December, 2019. This research was partly supported by National Natural Science Foundation of China (Grant No. 41876098 and Grant No. 81901734) and Overseas Cooperation Research Fund of Tsinghua Shenzhen International Graduate School. (Grant No. HW201808). (Corresponding author: Xiu Li and Yongbing Zhang)

Jiangpeng Yan is with Department of Automation, Tsinghua University, Beijing 100091, China.

Shuo Chen is with Center for Biomedical Imaging Research, Department of Biomedical Engineering, School of Medicine, Tsinghua University, Beijing 100091, China.

Xiu Li and Yongbing Zhang are with Tsinghua Shenzhen International Graduate School, Tsinghua University, Shenzhen 518055, China. (e-mail: li.xiu@sz.tsinghua.edu.cn, zhang.yongbing@sz.tsinghua.edu.cn)

researchers try using deep neural networks to find the better sparse representations for MR image reconstruction. As far as we know, deep convolutional neural network (CNN) is firstly introduced to CS-MRI by Wang et al. [10], where a three-layer CNN was trained with L2 loss between paired zero-filled and fully-sampled reconstruction MR images. Since then, significant progresses have been made by researchers to produce better reconstruction results for DL-based CS-MRI task including data-driven methods [11] [12] and model-driven methods [13] [14]. A detailed review will be introduced in the following section. Researchers have successfully developed various DL-based frameworks for CS-MRI, but not enough attention was paid to how the network architectures can affect MR image reconstruction results. In previous works, all the networks were designed by handcraft, thus the performances of these networks are limited by researchers expertise and labor naturally with the following two concerns. On one hand, only several common convolutional operations (e.g. 3×3 convolutional layer) are tried in current works and other operations (e.g. dilated convolution) with their possible combinations are not sufficiently explored. On the other hand, it is hard to balance the performance and computation cost of CNNs by manual attempts. Usually, the neural network consumes a significant number of computation resources and larger and deeper networks perform better but with heavy computation load. Therefore, DL-based CS-MRI methods can be not friendly for practical clinical translation.

In this manuscript, we introduce a novel DL-based framework for CS-MRI, and our main contributions can be summarized in three aspects as follows:

- We proposed a neural network architecture designed for CS-MRI task by differentiable neural architecture search (NAS) algorithm. The inner cells in our network are automatically searched from a pre-defined search space, allowing flexible combination of different operations. To our knowledge, we are the first to combine neural architecture search with CS-MRI for finding better sparse representations.
- Experiments performed on fastMRI dataset [15], a publicly available complex-valued MRI dataset collected from real MRI devices, demonstrate that our network achieves better performance with fewer computation resources than previous manual design architectures.
- We analyse the automatically found networks by extending experiments on internal network structure. The searched structures and the NAS workflow can offer insights to design neural networks for other medical image applications.

The organization of this paper is as follows. In Section II, recent developments of DL-based CS-MRI frameworks and NAS algorithms are reviewed. In Section III, details of how to automatically search the network architecture are elaborated. In Section IV, extensive experiments are conducted to verify the effectiveness of our network from both quantitative and qualitative perspective. In Section V, we discuss and draw the conclusion of this study.

II. RELATED WORK

A. Recent Developments in DL based CS-MRI frameworks

Current DL based CS-MRI frameworks can be roughly summarized into two categories: data-driven and model-driven methods.

For data-driven methods, inspired by the initial try of Wang et al. [10], researchers designed different networks to directly learn the mapping between different MRI related domains [16] [17]. Zhu et al. [11] proposed AutoMap method to reconstruct MR images from k-space data with fully-connected and convolutional layers. RAKI [18] and LORAKI [19] instead focused on using CNNs to implement interpolation reconstruction in k-space domain. Different generative adversarial networks (GAN) [20] were explored in [12] [21] and [22] to reconstruct MR images with a GAN-based loss for recovering more detailed textures. In these data-driven methods, deep networks can be regarded a “black box” from input to output and are trained in end-to-end way. There is no doubt that integrating traditional algorithms properly with deep networks can benefit reconstruction results, so model-driven methods are proposed.

For model-driven methods, researchers use deep neural networks to learn image priors, i.e. sparse representations for MR image reconstruction and then integrated these networks into traditional algorithms to unroll the iteration process. Sun et. al. [23] firstly used convolutional layers to unroll the Alternating Direction Method of Multipliers (ADMM) optimization to solve single-coil MR image reconstruction. A variational network was proposed by [24] to solve multi-coil MR image reconstruction problem. The data consistency module proposed in DCCNN [13] that performs iterative reconstruction in a cascading way has a great impact for following works [17] [25] [26]. The cascading data consistency constraint is then generalized for common inverse problems as model-based deep learning framework MoDL [14]. To some degree, DCCNN and MoDL share similarities with data-driven methods because the “black box CNN block is used as the “denoiser” in their frameworks and can be regarded as hybrid-driven methods [27].

Although there exist various reconstruction frameworks now, the network architectures used are very similar in both data-driven and model-driven methods. U-net [28] and its variants with residual learning [16], cascading n-fold architecture [22] or channel-wise attention [17] are explored independently. U-net is famous for its success in medical image semantic segmentation, but it is not designed specifically for MR image reconstruction. In [10] [13] [14] and [18], plain fully convolutional networks were adopted. Following DCCNN [13], RDN [25] introduced dilated convolution [29] and recursive learning [30] to produce higher quality MR images with fewer network parameters. [17] and [26] also focused on how to design fine and novel structures instead of plain CNN with data consistency module to improve reconstruction performance. These architectures are all human designed limited by the concerns mentioned above and the motivation of our work is finding the best architecture in an automatically search way.

B. Recent Developments in NAS Algorithms

The network architecture plays an important role in the study of DL and there exist many famous architectures, e.g. AlexNet [31], InceptionNet [32], ResNet [33], etc. NAS aims to develop algorithms for automatically neural architectures design. Recent works have successfully exceeded human designed ones on large-scale image classification [34] [35]. At a high level, current methods usually fall into three categories: evolutionary algorithm (EA) [36], reinforcement learning (RL) [37] differentiable search. In EA based NAS methods [38] and [39], the best architecture was obtained by progressively mutating a population of candidate architectures. Reinforcement learning (RL) techniques is an alternative to EA in [35] and [40] by training a recurrent neural network [41] meta-controller to generate final architectures from a predefined sequences encoding search space. The major limitation of these EA and RL based methods is that they tend to require a large amount of computation resources.

Our work is most closely related to the final differentiable search methods. Based on the continuous relaxation of the architecture representation [34], the architecture of inner cells can be selected via back propagation [42] automatically. Recent applications of differentiable search all focus on classification and segmentation task of natural images, typically DARTS [34] and Auto-Deeplab [43]. These works can search novel network architectures that perform better than previous handcrafted ones.

III. METHODOLOGY

To clarify our method, we first introduce the background for DL based MR image reconstruction framework, then we present our neural architecture search strategy.

A. DL Based MR Image Reconstruction Framework

We follow DCCNN [13] and MoDL [14] to unroll the alternating minimization algorithm with cascading CNN-derived constraint for CS-MRI problem by the following formulations.

We need to deal with complex numbers for MR images reconstruction. In this manuscript, equivalent real data x is used to represent complex data \tilde{x} of size $n_r \times n_c = N$ as follows:

$$\tilde{x} = x_{re} + jx_{im} \in \mathbb{C}^N \leftrightarrow x = [x_{re}, x_{im}] \in \mathbb{R}^{2N}. \quad (1)$$

The aim of CS-MRI is to reconstruct high-quality MR image x from sub-sample k-space measurement $s \in \mathbb{C}^M (M < N)$, such that:

$$s = Ux, \quad (2)$$

where $U \in \mathbb{C}^{M \times N}$ is the sub-sampling encoding matrix (e.g. Fourier encoding). Then x can be obtained by solving the following unconstrained optimization problem:

$$\min_x \|s - Ux\|_2^2 + \mathcal{R}(x), \quad (3)$$

where $\mathcal{R}(x)$ is the regularization term in image domain, while $\|s - Ux\|_2^2$ can be regard as the data consistence term between

image domain and k-space domain. For traditional CS-MRI framework, L1 and L2 norms in the specific domain of x is often used as the regularization term. For DL based CS-MRI, the deep CNN is integrated in this formulation by:

$$\min_x \|s - Ux\|_2^2 + \lambda \|x - \mathcal{D}(x, \omega)\|^2, \quad (4)$$

where \mathcal{D} represents the deep CNN network with learn-able weights ω . This problem can be solved with the alternating minimization algorithm by:

$$x^{(n+1)} = \arg \min_x \|s - Ux\|_2^2 + \lambda \|x - y^{(n)}\|^2 \quad (5)$$

$$y^{(n+1)} = \mathcal{D}(x^{(n+1)}, \omega). \quad (6)$$

The sub-problem of Eq.6 can be regarded as the de-aliasing problem in image domain. Given paired zero-filled MR reconstruction image as x and fully-sampled MR images y , the CNN \mathcal{D} with its weight weights ω can be obtained by minimizing the objective function:

$$\min_{\omega} \mathcal{L}(\mathcal{D}(x, \omega) - y), \quad (7)$$

where \mathcal{L} is the loss function, e. g. L1 loss or L2 loss.

The sub-problem of Eq.5 is related to the data consistency problem between k-space and image domain. Consider single channel MR image acquisition, i.e. $U = MF$ where $F \in \mathbb{C}^{N \times N}$ applies two-dimensional Fast Fourier Transform (FFT) and $M \in \mathbb{C}^{M \times N}$ is the sub-sampling mask selecting lines in k-space, such that Eq.5 has a close-formed solution:

$$x = (1 + \lambda U^T U)^{-1} (\mathcal{D}(x, \omega) + \lambda U^T s). \quad (8)$$

This solution is firstly introduced in DCCNN [13] as data consistency process. MoDL [14] generalized Eq.5 to multi-channel acquisition cases. E.g. for multi-coil MR image, we have $U = MFS$ where the coil sensitivity map S needs to be taken into consideration so the conjugate gradient (CG) algorithm is used to solve this more complex problem because $1 + \lambda U^T U$ is not analytically invertible. The data consistency process can then be integrated as a layer with deep CNNs without trainable parameters. In other degree, we fuse the accurate partial k-space data into deep CNNs to correct biases that accrue during the inference periods by Eq.8. Because multi-channel MRI data need a great number of computing resources, we perform all the formulations and experiments in single-coil MR image reconstruction scene following [15] [25] for demonstration purposes.

Note the deep CNNs by reconstruction module and the data consistency process by k-space data fusion module, we can unroll Eq.5 and Eq.6 by cascading modules. According to limited computation resource we have, we iterate these modules three times to form the final backbone shown in Fig. 2.

Under this uniform framework, there exist some works [17] [25] [26] discussing how the design of reconstruction module can improve the quality of MR image reconstruction. And as mentioned above, their networks are all built by handcraft. DCCNN [13] uses a plain CNN as the reconstruction module

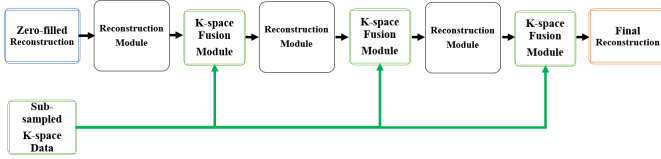


Fig. 2. The backbone framework of MR image reconstruction. The K-space Fusion Module helps to correct biases that accrue during the inference of the CNN. Similar strategy is used in different works including [13] [14] [17] [25] [26], with various reconstruction modules. In MoDL [14], reconstruction modules share the same weights to reduce learnable parameters.

with residual learning shown in Fig. 3. In MoDL [14], all the reconstruction modules share the same weights to reduce number of parameters. RDN [25] uses a recursive dilated network instead shown in Fig. 4. In this work, we use neural architecture search algorithm to search and design the reconstruction module automatically.

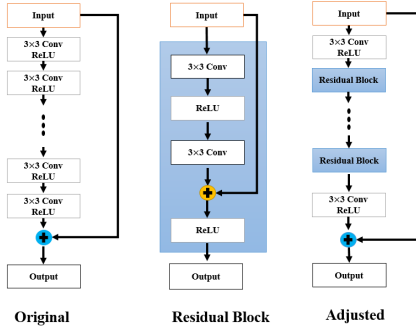


Fig. 3. The reconstruction module of DCCNN [13] and MoDL [14]. Plain convolutional neural network with residual learning is adopted originally drawn in the left. In our re-implementation, we use residual blocks instead of plain CNN drawn in the right.

B. Differentiable Search Strategy

The introduction of differentiable search strategy starts from concept of *cell*.

1) *Cell Level Search*: We reuse the concept of *cell*, which is also adopted in [34] [43] [44]. The *cell* acts as the micro building block which can be stacked to form a deeper network. In this manuscript, a cell maps the output tensors of previous two cells to construct its own output, i.e. note the output of cell l by C_l , we can have:

$$C_l = \text{Cell}(C_{l-1}, C_{l-2}, \alpha), \quad (9)$$

where α is a parameter representing the relaxation of discrete inner cell architectures by the following formulations.

The inner cell architecture of cell l can be defined as a directed acyclic computation graph formed by sequential internal nodes $[P_l^1, P_l^2, \dots, P_l^n]$ shown in Fig. 5. Note the output of P_l^i by C_l^i , we have:

$$C_l = \text{Concat}(C_l^1, C_l^2, \dots, C_l^n). \quad (10)$$

Define the connections between two nodes as a selection from candidate layer operations set \mathcal{O} , the input of P_l^i as a selection

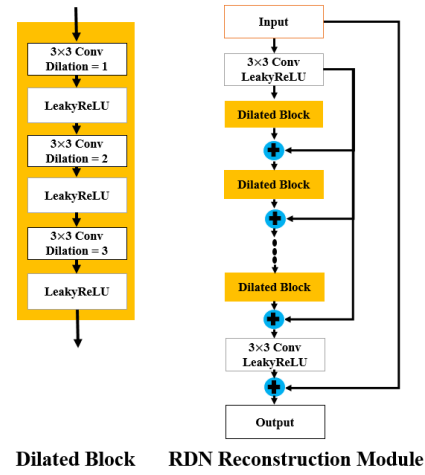


Fig. 4. The reconstruction module of RDN [25]. Dilated convolution is used to expand perception field and improve the performance. And the yellow dilated blocks share the same weights in reconstruction module by recursive learning [30] to reduce parameters.

from tensors set \mathcal{I}_l^i . \mathcal{O} contains different CNN layer types, e. g. 3×3 convolutional layers. The latter node can take in the input of this cell and all previous nodes' output, so we have: $\mathcal{I}_l^1 = [C_{l-1}, C_{l-2}]$, $\mathcal{I}_l^2 = [C_{l-1}, C_{l-2}, C_l^1]$, $\mathcal{I}_l^3 = [C_{l-1}, C_{l-2}, C_l^1, C_l^2]$, \dots .

Before searching internal cell architecture, these nodes are densely connected by all possible layer types in \mathcal{O} with the operation weight α shown in the left of Fig. 5. The parameter α can be defined and integrated into each cell node by the following two steps.

First, the output of P_l^i is defined by tensors in \mathcal{I}_l^i , we have:

$$C_l^i = \sum_{I_l^j \in \mathcal{I}_l^i} O_{j \rightarrow i}(I_l^j), \quad (11)$$

Second, parameter α is added as the probability associated with each operation $O^k \in \mathcal{O}$ by:

$$O_{j \rightarrow i}(I_l^j) = \sum_{O^k \in \mathcal{O}} \alpha_{j \rightarrow i}^k O^k(I_l^j), \quad (12)$$

where α is limited by:

$$\sum_{k=1}^{|\mathcal{O}|} \alpha_{j \rightarrow i}^k = 1, \forall i > j, \quad (13)$$

$$\alpha_{j \rightarrow i}^k \geq 0, \forall i > j, O^k \in \mathcal{O}. \quad (14)$$

With such definition of α , the cell search problem can be successfully integrated into an differentiable computation graph. After optimizing α via gradient decent, the layer operations with top-2 α -value are preserved to form the final structure shown in the right of Fig. 5.

2) *Operations Search Space Design*: The candidate layer operations set \mathcal{O} is defined by us as follows shown in Fig. 6:

- Sep_Conv_3x3 : 3×3 separable convolutional layer is formed by cascading 3×3 depthwise separable convolutional layer and 1×1 pointwise layer.
- Dil_2_Conv_3x3 : 3×3 separable convolutional layer with dilation rate 2 in depthwise separable layer.

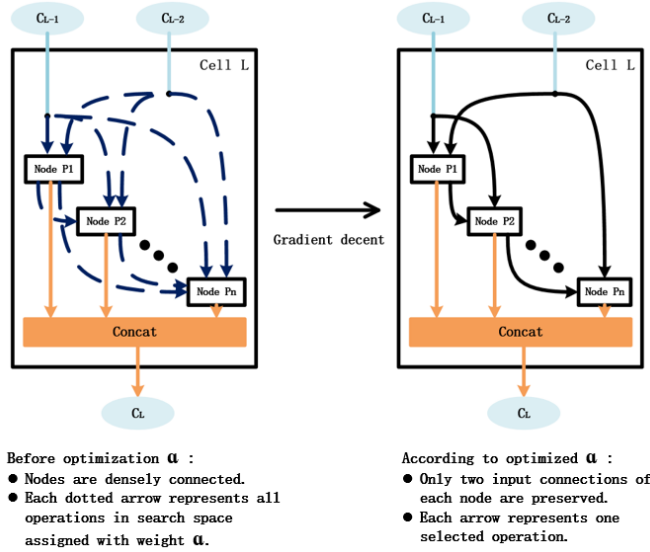


Fig. 5. The cell takes in the output tensors of previous two cells to construct its own output. Internal nodes with connections formed the cell are defined as a directed acyclic computation graph. Before architecture search, these nodes are densely connected by all possible layer types shown in the left. After gradient decent, the best two connections with its most suitable layer type are preserved according to α and form the final architecture in the right.

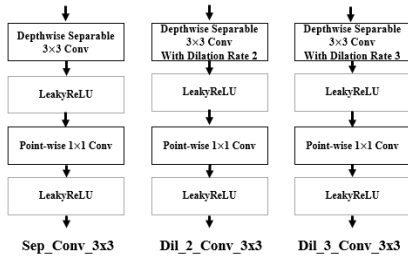


Fig. 6. The candidate layer operations set \mathcal{O} .

- Dil_3_Conv_3x3 : 3×3 separable convolutional layer with dilation rate 3 in depthwise separable layer.
- Skip connect
- None connect

We choose these operations based on the following observation and summary of previous works:

- Separable convolution is proposed by [45] and widely used in Mobilenet [46], Shufflenet [47] and other efficient networks. Comparing with common convolutional layer, separable convolution can use fewer calculations and parameters.
- MR image reconstruction problem can be considered as a de-aliasing task belonging to low-level image processing. Reference [48] proved that removing batch-normalization [49] helps to improve results. So we do not use normalization in all the layers.
- Dilated convolution [29] is also widely adopted in low-level image analysis tasks, because it can expand perception field without adding parameters. RDN [25] shows that dilated layers with various dilation rates benefit the performance of CS-MRI.

It is also worth to mention that convolutional layers in our network are all no-bias. We adopt no-bias convolutional layers according to the following consideration. As mentioned above, paired zero-filled MR image x and fully-sampled MR image y are complex-valued, and the phases of complex numbers are meaningful. If convolutional layers have biases, it will be more difficult to keep the phases because:

$$\frac{Wx_{re}}{Wx_{im}} \neq \frac{Wx_{re} + b}{Wx_{im} + b}, \quad (15)$$

where W represents weight and b represents bias of convolutional layers.

3) *Module Level Structure Design*: After explanation of cell structure and the operations search space, we stack cells to build our reconstruction module drawn in Fig. 7.

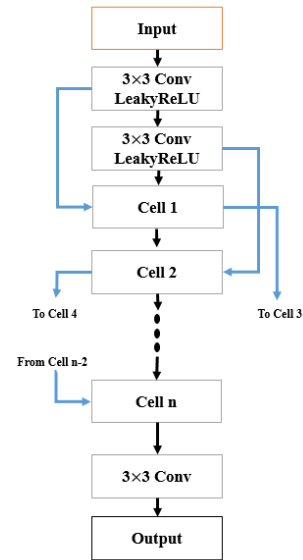


Fig. 7. The reconstruction module used in our network. The two convolutional layers in the beginning is used to expand channel number of input data. The final layer is used to produce output. The automatically searched cells are stacked to form the whole architecture.

The first and second common 3×3 convolutional layers are used to expand channels of two-channel input data and the final 3×3 convolutional layer is also designed to produce two-channel output.

4) *Optimization Strategy*: Since the reconstruction module is built, we follow the optimization strategy in [34] to search the inner structure of cells. We divide the training data into two disjoint sets train_{ω} and train_{α} according to the first-order approximation. The disjoint set partition also prevents the architecture from over-fitting the whole training data.

The optimization alternates between:

1. Update network weights ω by $\nabla_{\omega} \mathcal{L}_{\text{train}_{\omega}}(\omega, \alpha)$,
2. Update architecture α by $\nabla_{\alpha} \mathcal{L}_{\text{train}_{\alpha}}(\omega, \alpha)$.

The optimization object function $\mathcal{L}(\omega, \alpha)$ is defined by integrating α to Eq.7 as:

$$\min_{\omega} \mathcal{L}(\mathcal{D}(x, \omega, \alpha) - y). \quad (16)$$

According to [50], L1 loss is beneficial to train machine learning models on computer vision tasks, even when the

evaluation is performed under L2 norm related metrics, e.g. PSNR. Inspired by this, we define the loss function \mathcal{L} as L1 loss between paired zero-filled MR image x and fully-sampled MR image y . The searching process needs to be stopped when the cell structure starts to keep stable according to early stopping strategy, which is commonly used in NAS works [51] [52].

To clarify the final searched cell structure, we can define a 4-tuple $P_l^i = [I_l^{i1}, I_l^{i2}, O_l^{i1}, O_l^{i2}]$, where $I_l^{i1}, I_l^{i2} \in \mathcal{I}_l^i$ are selections of the input tensors and $O_l^{i1}, O_l^{i2} \in \mathcal{O}$ are selections of candidate layer operations based on the optimized α value. Thus we have:

$$C_l^i = O_l^{i1}(I_l^{i1}) + O_l^{i2}(I_l^{i2}). \quad (17)$$

Finally, the structure of cell is defined and can then be used as common CNN module. In other words, we sampled a smaller but most important architecture from a densely connected large network according to optimized α . Given a pre-searched architecture with N cells and M internal nodes for each and operations search space contains J types, we can use the number of total operations in this computation graph to approximate computation graph complexity, thus we have:

$$N \times \frac{(M+3)M}{2} \times J \rightarrow N \times 2M \times 1. \quad (18)$$

After the structure of the whole network is found, the final network needs to be re-trained on the whole training set to maximize its final reconstruction performance.

IV. EXPERIMENTAL ANALYSES

We compare our framework with the following methods: conventional Total Variation (TV) [53] minimization based iteration algorithm, U-net baseline model used in [15] as typically data-driven method, DCCNN [13], MoDL [14] and RDN [25] which can be regarded as a representative improved approach following DCCNN and MoDL.

A. Dataset and Data Pre-processing

We conduct all the experiments on fastMRI dataset [15] which contains raw MR measurements of knees from real clinical scans. There are 1594 patients with around 50000 slices and occupies more than 120GB storage space in the whole dataset. Due to limited computation resources we have, we randomly selected 80 scans with 2829 MR slices as training set and 40 scans with 1457 slices as testing set from single-coil data, and this mini-fastMRI dataset contains more slices than experiments in DCCNN [13] and RDN [25].

The data in mini-fastMRI dataset are raw complex-valued fully-sampled k-space data with different sizes, thus the following steps are performed to make paired 320×320 zero-filled and fully-sampled reconstructions: First, 2D-IFFT is applied on original k-space data to get MR images, which are then cropped centrally to become 320×320 patches. After that, 2D-FFT is performed on each patch and obtain corresponding 320×320 fully-sampled k-space data. To simulate accelerated signals acquisition process, we use 4-fold and 8-fold Cartesian

sub-sampling mask following the setting provided by [15]. When acceleration factor equals 4, the fully-sampled central region includes 8% k-space lines, while when acceleration factor equals 8, 4% k-space lines are sampled, and the remaining k-space lines are included uniformly at random. After applying such masks on fully-sampled k-space data, we can get the zero-filled reconstruction by 2D-IFFT.

We take the complex-valued MR image as 2-channel real-valued image as mentioned above. Before feeding MR images to deep networks, we normalize the data to $[-6, 6]$ with constant phase.

B. Implementation Details

We use the BART toolkit [54] to estimate ESPIRiT coil sensitivity and perform TV reconstruction algorithm. We set the total variation regularization weight as 0.01 and implement 200 iterations on each slice.

All the deep CNNs in this manuscript are implemented with Pytorch [55] and trained on one TITAN X Pascal GPU with 12GB memory. The input and output of all the CNNs are 2 channels. No normalization operation is used in these networks.

We search our reconstruction module with 3 cascading cells and each cell includes 3 internal computation nodes. The final searched cell structure is drawn in Fig. 8. The outputs of C_{l-1} and C_{l-2} are processed by 1×1 convolutional layers to reduce channels number from 96 to 32.

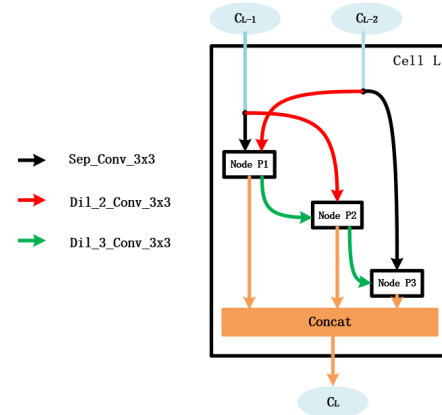


Fig. 8. The final searched cell structure with 3 internal nodes. Two input connections with their independent layer type are preserved to form the whole architecture.

To make different networks comparable, we try our best to balance the computing resources of different networks. For all the networks, the FLOPs of one inference are calculated by counting multiplication and add operations in all convolutional layers in reconstruction modules after feeding a 320×320 2-channel MR image into the networks. As a result, the reconstruction module of DCCNN [13] contains 3 residual blocks, and the reconstruction module of RDN [25] contains 3 recursive dilated blocks to have comparable FLOPs and parameters like our searched networks. Because we are dealing with single-coil reconstruction, we can retrain the DCCNN with sharing-weight reconstruction modules to re-implement

MoDL [14]. For U-net, the input data are down-sampled 4 times with channels doubled starting from 32 channels. And all the other networks have 32-channels layers.

According to DCCNN [13] and RDN [25], more blocks in their networks will produce better results. Thus, we also add more blocks in these networks to evaluate whether they can use more computation resources to achieve similar performance with our searched network.

We use Adam optimizer [56] for parameter learning with L1 loss only. The initial learning rate is set to be 0.001 for the first 40 epochs and 0.0001 for the later 40 epochs for all the networks in the training set. During training and testing process, the 4-fold and 8-fold Cartesian sub-sampling mask is generated randomly for every slice with equal possibility. This can also be viewed as a data augmentation to avoid over-fitting [57].

We evaluate the MSE, Normalized MSE (NMSE), PSNR and SSIM [58] between reconstructed results and fully-sampled target MR images on modulus to compare with other works.

C. Reconstruction Results Comparison

The quantitative evaluation results are shown in Table I, demonstrating that our proposed network outperforms current state-of-the-art frameworks. Half of total slices are sub-sampled with 4-fold Cartesian sub-sampling masks and the other with 8-fold ones. All quantitative evaluation results are calculated on images reconstructed from the same corresponding sub-sampling data.

Among comparison experiments, U-net is more different with other deep learning models listed in this table, because the feature maps are reduced in size after down-sampling with channels doubled. So U-net has much more learnable parameters than others with fewer operations. U-net has $40\times$ more parameters than our proposed network without providing better results.

DCCNN, MoDL, RDN and our network all adopt k-space fusion strategy. Comparing to DCCNN, MoDL uses sharing-weight reconstruction modules to reduce parameters and leads to worse reconstruction results. Because dilated blocks in RDN share the same weight, so its learnable parameters do not increase with number of blocks. Although RDN and MoDL uses fewer learnable parameters, “there is no free lunch”, the FLOPs do not decrease by recursive learning, i.e. the inference speed is still limited. Our automatically searched network architecture uses $4\times$ fewer FLOPs to reconstruct better results than RDN with 8 recursive dilated blocks.

The qualitative evaluation results of all the methods are shown in Fig. 9. We present two slices reconstructed from different sub-sampling ratios. Our network can reduce aliasing pattern more effectively comparing with other methods. When the sub-sampling ration gets bigger, our model performs much better than other methods. Structural details in our MR reconstruction images are much more accurate.

D. Experiments on the Number of Internal Nodes

Although the architecture of cells are searched automatically, the number of internal nodes are still a hyper-parameter

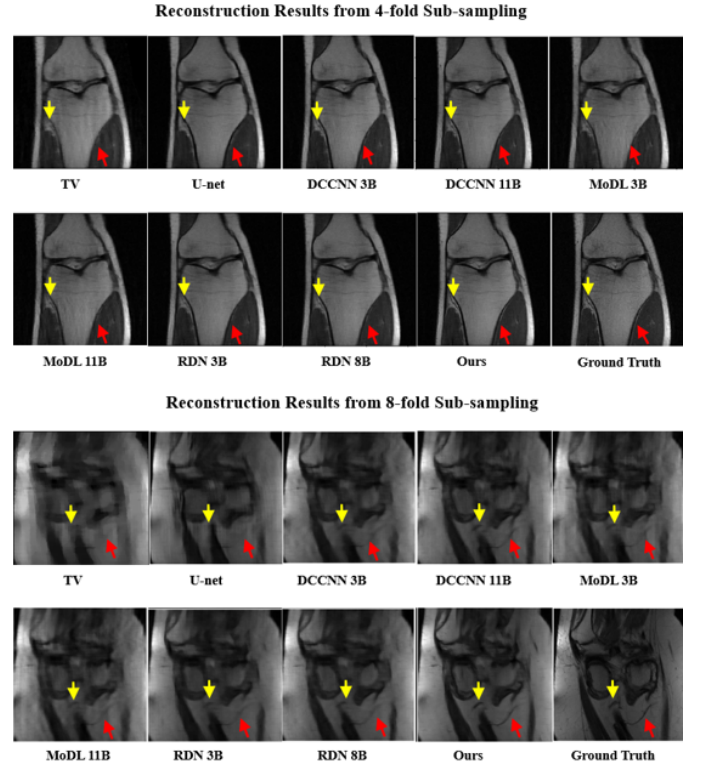


Fig. 9. The qualitative evaluation results of all the methods. We present two slices reconstructed from different sub-sampling ratio. Here the arrows point show that our reconstruction results offer more details similar to ground truth while other methods fail.

set by human. In this part, we conduct experiments to search reconstruction module with 3 cascading cells and each cell includes different number of internal nodes. The searched results with 2 and 4 internal nodes are drawn in Fig. 10. The reconstruction results of these architectures are listed in Table II.

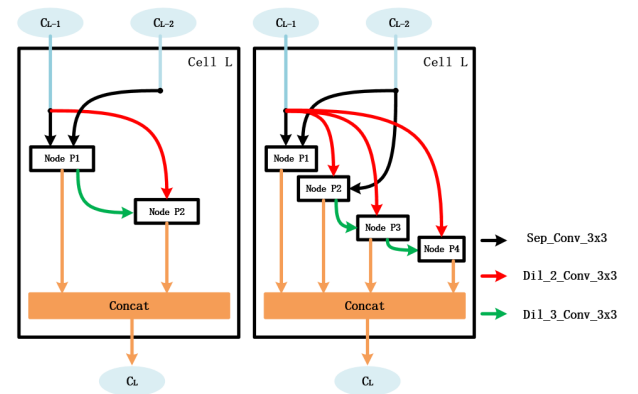


Fig. 10. The searched structures of cell with 2 and 4 internal nodes number. Convolutional layers with larger perception field are always placed in the bottom and Feature maps from different levels are fused properly. By observing the selection of connections and layer types, some insights of network design can be concluded.

The found structures demonstrate that the algorithm do learn some principles to form the reconstruction architecture automatically. These principles offer insights for other researchers to design their network for other low-level medical image

TABLE I
QUANTITATIVE EVALUATION RESULTS OF ALL THE METHODS ($AVG \pm STD$)

| Model | MSE ($\times 1e-10$) | NMSE ($\times 1e-2$) | PSNR | SSIM | FLOPs | Params. |
|-------------------------------------|-------------------------------------|-------------------------------------|-------------------------------------|---------------------------------------|--------|---------|
| TV | 2.351 ± 5.355 | 7.104 ± 7.633 | 28.12 ± 6.246 | 0.5192 ± 0.2509 | | |
| U-net | 1.764 ± 3.742 | 5.654 ± 6.321 | 29.15 ± 5.904 | 0.6028 ± 0.2508 | 12.17G | 3349K |
| DCCNN with 3 residual blocks | 1.718 ± 4.021 | 5.521 ± 6.484 | 29.37 ± 6.538 | 0.6118 ± 0.2648 | 17.41G | 170.0K |
| DCCNN with 11 residual blocks | 1.635 ± 3.651 | 5.407 ± 6.456 | 29.49 ± 6.544 | 0.6147 ± 0.2658 | 62.87G | 613.9K |
| MoDL with 3 residual blocks | 2.025 ± 5.167 | 5.886 ± 6.358 | 28.95 ± 6.226 | 0.6075 ± 0.2596 | 17.41G | 56.7K |
| MoDL with 11 residual blocks | 1.938 ± 4.785 | 5.788 ± 6.356 | 29.04 ± 6.235 | 0.6089 ± 0.2606 | 62.87G | 204.3K |
| RDN with 3 recursive dilated blocks | 1.623 ± 3.587 | 5.398 ± 6.444 | 29.49 ± 6.501 | 0.6147 ± 0.2656 | 26.03G | 86.79K |
| RDN with 8 recursive dilated blocks | 1.531 ± 3.204 | 5.290 ± 6.468 | 29.62 ± 6.534 | 0.6170 ± 0.2665 | 68.79G | 86.79K |
| Ours | 1.432 ± 2.919 | 5.112 ± 6.408 | 29.83 ± 6.692 | 0.6204 ± 0.2676 | 15.07G | 142.3K |

TABLE II
QUANTITATIVE EVALUATION RESULTS OF SEARCHED ARCHITECTURES WITH DIFFERENT INTERNAL NODES. ($AVG \pm STD$)

| Number of Nodes | MSE ($\times 1e-10$) | NMSE ($\times 1e-2$) | PSNR | SSIM | FLOPs | Params. |
|-----------------|------------------------|------------------------|-------------------|---------------------|--------|---------|
| 2 | 1.462 ± 3.046 | 5.148 ± 6.407 | 29.78 ± 6.696 | 0.6201 ± 0.2684 | 11.37G | 107.7K |
| 3 | 1.432 ± 2.919 | 5.112 ± 6.408 | 29.83 ± 6.692 | 0.6204 ± 0.2676 | 15.07G | 142.3K |
| 4 | 1.405 ± 2.781 | 5.081 ± 6.420 | 29.87 ± 6.719 | 0.6218 ± 0.2687 | 18.76G | 176.8K |

tasks, e. g. Semantic Segmentation or Super Resolution:

- Deeper feature maps require larger perception field. In our searched results, layers with dilation rate 3 are always preferred in the bottom of the cell behind layers with dilation rate 2.
- It is important to fuse feature maps from different levels properly. In our searched cell structure, feature maps from C_{l-2} are used to refine different nodes.
- The number of convolutional layers, i. e. the complexity of structure, needs to be controlled. When we make each cell include 4 nodes, Node 1 is disconnected from other nodes in the search result shown in Fig. 10 indicating that more computing nodes might be redundant.

E. Experiments on the Operations Search Space

In this part, expanding experiment are conducted to find the relationship between operations search space and network performance.

Note original operations search space by A, we define a new space B as follows:

- Sep_Conv_3x3
- Dil_2_Conv_3x3
- Conv_9x1_1x9 : two cascading depthwise separable convolutional layers with kernel size 9×1 and 1×9 .
- Skip Connect
- None Connect

The design of Conv_9x1_1x9 shown in Fig. 11 is inspired by [59], where large convolutional kernels lead to better performance in semantic segmentation. Two cascading 9×1 and 1×9 convolutional layers enables dense connections within a large 9×9 region when producing the feature map.

The search result is drawn in Fig. 12 and the reconstruction results of these architectures are listed in Table III. It is shown that with a different search space, the new searched architecture uses fewer parameters to provide similar performance. We can conclude that the proper connections searched play a more important role in MR image reconstruction than layer types. And the principle that larger perception layers are placed in

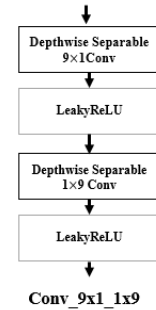


Fig. 11. The structure of Conv_9x1_1x9. Two cascading convolutional layers with 9×1 and 1×9 kernel size are adopted to achieve a 9×9 perception field.

the bottom still holds. What's more, the setting of layer types allow us to explore more possibilities, if there are some novel and efficient layer types proposed in the future.

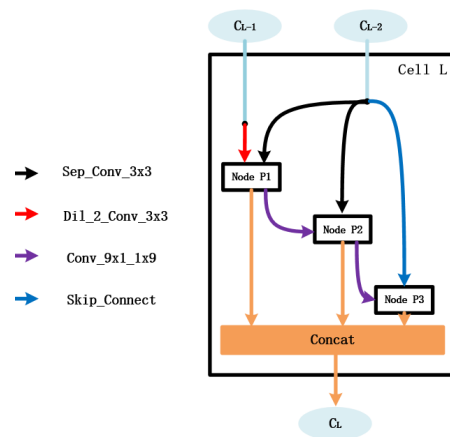


Fig. 12. The searched cell structure when the operations search space is redefined.

V. DISCUSSION AND CONCLUSION

The MRI acceleration is highly demanded in clinical practice and has been an active research area for years. The

TABLE III

QUANTITATIVE EVALUATION RESULTS OF SEARCHED ARCHITECTURES WITH DIFFERENT OPERATIONS SEARCH SPACES. ($AVG \pm STD$)

| Operations Search Space | MSE ($\times 1e-10$) | NMSE ($\times 1e-2$) | PSNR | SSIM | FLOPs | Params. |
|-------------------------|------------------------|------------------------|-------------------|---------------------|--------|---------|
| A | 1.432 ± 2.919 | 5.112 ± 6.408 | 29.83 ± 6.692 | 0.6204 ± 0.2676 | 15.07G | 142.3K |
| B | 1.439 ± 2.935 | 5.122 ± 6.401 | 29.81 ± 6.693 | 0.6202 ± 0.2678 | 12.44G | 117.2K |

introduction of compressed sensing (CS) in 2006 [4] made a significant breakthrough in the reduction of MRI scan time. Nowadays, the deep learning technology brings new chances for us to solve this problem better. Although plenty of works have been explored [13] [14], there still exists a gap between research works and clinical practice due to complex network architecture design and heavy computation cost. In this work, we evaluate the applicability of NAS to improve the DL based CS-MRI performance remarkably. The key insight of our work is that we can search a specific and novel network architecture for CS-MRI in a differentiable way, based on continuous relaxation of cell. The setting of layer types in cell's operations searching space makes it an open workflow allowing us to inherit other good fine structure design to form new architectures. It is worth to mention that this workflow can also be generalized to multi-coil MRI data easily because we share similar framework with MoDL [14]. Experiments on a publicly available dataset demonstrate that our optimized network can reconstruct MR images better than previous handcrafted networks with 4 times fewer computation resources. The automatically searched neural architecture balances performance and efficiency more properly than human experts. And with faster and better reconstruction results, our method is more friendly for clinical translation. Extensive experiments about number of internal nodes show that the network architectures found by NAS algorithm follow some basic principles, offering insights for networks used in other low-level medical image tasks.

Although the internal cell of our network can be searched automatically, the module-level architecture is still defined by human experience. There are many hyper parameters remaining in our method, e. g. numbers of internal nodes, numbers of cells in macro module, kernel size of convolutional layer, etc. Therefore, we will try to address this problem by exploring the usage of the reinforcement learning techniques [37] [60] to set these parameters instead of humans. Also we only use L1 loss function to supervise all deep models in our experiments. Reference [21] and [22] introduce combined loss functions for MR image reconstruction and produce better results. More efforts will be involved to extend this neural architecture search framework with more effective loss function in the near future.

To conclude, we present a novel reconstruction network for CS-MRI task by searching the network architecture automatically. Experiments show the searched network can reconstruct MR images better and more efficiently than previous works. With the superiority of good performance and the general applicability of neural architecture search, we expect that the proposed workflow can potentially be extended to other medical image applications.

ACKNOWLEDGMENT

The authors would like to thank Dr Zechen Zhou, Philips Research North America, Cambridge, Massachusetts, and Dr Rui Li, Center for Biomedical Imaging Research, Department of Biomedical Engineering, School of Medicine, Tsinghua University for their valuable discussions that significantly improved the quality of the manuscript. They also thank the authors of fastMRI [15] for making thToo many commas in nameeir code and dataset accessible online.

REFERENCES

- [1] Z.-P. Liang and P. C. Lauterbur, *Principles of magnetic resonance imaging: a signal processing perspective*. SPIE Optical Engineering Press, 2000.
- [2] J. Tsao and S. Kozerke, "Mri temporal acceleration techniques," *Journal of Magnetic Resonance Imaging*, vol. 36, no. 3, pp. 543–560, 2012.
- [3] M. Lustig, D. L. Donoho, J. M. Santos, and J. M. Pauly, "Compressed sensing mri," *IEEE signal processing magazine*, vol. 25, no. 2, p. 72, 2008.
- [4] D. L. Donoho, "Compressed sensing," *IEEE Transactions on Information Theory*, vol. 52, no. 4, pp. 1289–1306, 2006.
- [5] Y. LeCun, Y. Bengio, and G. Hinton, "Deep learning," *Nature*, vol. 521, no. 7553, p. 436, 2015.
- [6] R. Girshick, J. Donahue, T. Darrell, and J. Malik, "Rich feature hierarchies for accurate object detection and semantic segmentation," in *IEEE Conference on Computer Vision and Pattern Recognition*, 2014.
- [7] J. Long, E. Shelhamer, and T. Darrell, "Fully convolutional networks for semantic segmentation," in *CVPR*, 2015.
- [8] J. Xie, L. Xu, and E. Chen, "Image denoising and inpainting with deep neural networks," in *International Conference on Neural Information Processing Systems*, 2012.
- [9] C. Dong, C. C. Loy, K. He, and X. Tang, "Image super-resolution using deep convolutional networks," *IEEE Transactions on Pattern Analysis and Machine Intelligence*, vol. 38, pp. 295–307, 2014.
- [10] S. Wang, Z. Su, L. Ying, P. Xi, S. Zhu, L. Feng, D. Feng, and L. Dong, "Accelerating magnetic resonance imaging via deep learning," in *IEEE International Symposium on Biomedical Imaging*, 2016.
- [11] B. Zhu, J. Z. Liu, S. F. Cauley, B. R. Rosen, and M. S. Rosen, "Image reconstruction by domain-transform manifold learning," *Nature*, vol. 555, no. 7697, p. 487, 2018.
- [12] M. Mardani, E. Gong, J. Y. Cheng, S. S. Vasanawala, G. Zaharchuk, L. Xing, and J. M. Pauly, "Deep generative adversarial neural networks for compressive sensing mri," *IEEE transactions on medical imaging*, vol. 38, no. 1, pp. 167–179, 2018.
- [13] J. Schlemper, J. Caballero, J. V. Hajnal, A. N. Price, and D. Rueckert, "A deep cascade of convolutional neural networks for dynamic mr image reconstruction," *IEEE Transactions on Medical Imaging*, vol. 37, pp. 491–503, 2017.
- [14] H. K. Aggarwal, M. P. Mani, and M. Jacob, "Modl: Model-based deep learning architecture for inverse problems," *IEEE transactions on medical imaging*, vol. 38, no. 2, pp. 394–405, 2018.
- [15] J. Zbontar, F. Knoll, A. Sriram, M. J. Muckley, M. Bruno, A. De-fazio, M. Parente, K. Geras, J. Katsnelson, H. Chandarana, Z. Zhang, M. Drozdal, A. Romero, M. G. Rabbat, P. Vincent, J. Pinkerton, D. Wang, N. Yakubova, E. Owens, C. L. Zitnick, M. P. Recht, D. K. Sodickson, and Y. W. Lui, "fastmri: An open dataset and benchmarks for accelerated mri," *ArXiv*, vol. abs/1811.08839, 2018.
- [16] D. Lee, J. J. Yoo, and J. C. Ye, "Deep residual learning for compressed sensing mri," *2017 IEEE 14th International Symposium on Biomedical Imaging (ISBI 2017)*, pp. 15–18, 2017.
- [17] Q. Huang, D. Yang, P. Wu, H. Qu, J. Yi, and D. N. Metaxas, "Mri reconstruction via cascaded channel-wise attention network," *16th IEEE 16th International Symposium on Biomedical Imaging (ISBI 2019)*, pp. 1622–1626, 2018.

- [18] M. Akçakaya, S. Moeller, S. Weingärtner, and K. Uğurbil, "Scan-specific robust artificial-neural-networks for k-space interpolation (raki) reconstruction: Database-free deep learning for fast imaging," *Magnetic resonance in medicine*, vol. 81, no. 1, pp. 439–453, 2019.
- [19] T. H. Kim, P. Garg, and J. P. Haldar, "Loraki: Autocalibrated recurrent neural networks for autoregressive mri reconstruction in k-space," *arXiv preprint arXiv:1904.09390*, 2019.
- [20] I. J. Goodfellow, J. Pouget-Abadie, M. Mirza, X. Bing, D. Warde-Farley, S. Ozair, A. Courville, and Y. Bengio, "Generative adversarial nets," in *International Conference on Neural Information Processing Systems*, 2014.
- [21] G. Yang, S. Yu, H. Dong, G. Slabaugh, P. L. Dragotti, X. Ye, F. Liu, S. Arridge, J. Keegan, and Y. Guo, "Dagan: Deep de-aliasing generative adversarial networks for fast compressed sensing mri reconstruction," *IEEE Transactions on Medical Imaging*, vol. 37, no. 6, pp. 1310–1321, 2017.
- [22] T. M. Quan, T. Nguyen-Duc, and W.-K. Jeong, "Compressed sensing mri reconstruction using a generative adversarial network with a cyclic loss," *IEEE Transactions on Medical Imaging*, vol. 37, pp. 1488–1497, 2018.
- [23] J. Sun, H. Li, Z. Xu *et al.*, "Deep admm-net for compressive sensing mri," in *Advances in neural information processing systems*, 2016, pp. 10–18.
- [24] K. Hammernik, T. Klatzer, E. Kobler, M. P. Recht, D. K. Sodickson, T. Pock, and F. Knoll, "Learning a variational network for reconstruction of accelerated mri data," *Magnetic resonance in medicine*, vol. 79, no. 6, pp. 3055–3071, 2018.
- [25] L. Sun, Z. Fan, Y. Huang, X. Ding, and J. W. Paisley, "Compressed sensing mri using a recursive dilated network," in *AAAI*, 2018.
- [26] K. Zeng, Y. Yang, G. Xiao, and Z. Chen, "A very deep densely connected network for compressed sensing mri," *IEEE Access*, vol. 7, pp. 85 430–85 439, 2019.
- [27] D. Liang, J. Cheng, Z. Ke, and L. Ying, "Deep mri reconstruction: Unrolled optimization algorithms meet neural networks," *arXiv preprint arXiv:1907.11711*, 2019.
- [28] O. Ronneberger, P. Fischer, and T. Brox, "U-net: Convolutional networks for biomedical image segmentation," in *International Conference on Medical Image Computing and Computer-assisted Intervention*, 2015.
- [29] F. Yu and V. Koltun, "Multi-scale context aggregation by dilated convolutions," *ArXiv*, vol. abs/1511.07122, 2015.
- [30] J. Kim, J. K. Lee, and K. M. Lee, "Deeply-recursive convolutional network for image super-resolution," *2016 IEEE Conference on Computer Vision and Pattern Recognition (CVPR)*, pp. 1637–1645, 2015.
- [31] A. Krizhevsky and G. Hinton, "Convolutional deep belief networks on cifar-10," *Unpublished manuscript*, vol. 40, no. 7, pp. 1–9, 2010.
- [32] C. Szegedy, S. Ioffe, V. Vanhoucke, and A. A. Alemi, "Inception-v4, inception-resnet and the impact of residual connections on learning," in *Thirty-First AAAI Conference on Artificial Intelligence*, 2017.
- [33] K. He, X. Zhang, S. Ren, and S. Jian, "Deep residual learning for image recognition," in *IEEE Conference on Computer Vision and Pattern Recognition*, 2016.
- [34] H. Liu, K. Simonyan, and Y. Yang, "Darts: Differentiable architecture search," *arXiv preprint arXiv:1806.09055*, 2018.
- [35] B. Zoph and Q. V. Le, "Neural architecture search with reinforcement learning," *arXiv preprint arXiv:1611.01578*, 2016.
- [36] P. J. Angeline, G. M. Saunders, and J. B. Pollack, "An evolutionary algorithm that constructs recurrent neural networks," *IEEE transactions on Neural Networks*, vol. 5, no. 1, pp. 54–65, 1994.
- [37] R. S. Sutton, A. G. Barto *et al.*, *Introduction to reinforcement learning*. MIT press Cambridge, 1998, vol. 2, no. 4.
- [38] E. Real, S. Moore, A. Selle, S. Saxena, Y. L. Suematsu, J. Tan, Q. V. Le, and A. Kurakin, "Large-scale evolution of image classifiers," in *Proceedings of the 34th International Conference on Machine Learning-Volume 70*. JMLR. org, 2017, pp. 2902–2911.
- [39] E. Real, A. Aggarwal, Y. Huang, and Q. V. Le, "Regularized evolution for image classifier architecture search," in *Proceedings of the AAAI Conference on Artificial Intelligence*, vol. 33, 2019, pp. 4780–4789.
- [40] C. Liu, B. Zoph, M. Neumann, J. Shlens, W. Hua, L.-J. Li, L. Fei-Fei, A. Yuille, J. Huang, and K. Murphy, "Progressive neural architecture search," in *Proceedings of the European Conference on Computer Vision (ECCV)*, 2018, pp. 19–34.
- [41] T. Mikolov, M. Karafiát, L. Burget, J. Černocký, and S. Khudanpur, "Recurrent neural network based language model," in *Eleventh annual conference of the international speech communication association*, 2010.
- [42] Y. LeCun, B. E. Boser, J. S. Denker, D. Henderson, R. E. Howard, W. E. Hubbard, and L. D. Jackel, "Handwritten digit recognition with a back-propagation network," in *NIPS*, 1989.
- [43] C. Liu, L.-C. Chen, F. Schroff, H. Adam, W. Hua, A. L. Yuille, and L. Fei-Fei, "Auto-deeplab: Hierarchical neural architecture search for semantic image segmentation," in *Proceedings of the IEEE Conference on Computer Vision and Pattern Recognition*, 2019, pp. 82–92.
- [44] H. Pham, M. Y. Guan, B. Zoph, Q. V. Le, and J. Dean, "Efficient neural architecture search via parameter sharing," *arXiv preprint arXiv:1802.03268*, 2018.
- [45] F. Chollet, "Xception: Deep learning with depthwise separable convolutions," in *Proceedings of the IEEE conference on computer vision and pattern recognition*, 2017, pp. 1251–1258.
- [46] A. G. Howard, M. Zhu, B. Chen, D. Kalenichenko, W. Wang, T. Weyand, M. Andreetto, and H. Adam, "Mobilenets: Efficient convolutional neural networks for mobile vision applications," *arXiv preprint arXiv:1704.04861*, 2017.
- [47] X. Zhang, X. Zhou, M. Lin, and J. Sun, "Shufflenet: An extremely efficient convolutional neural network for mobile devices," in *Proceedings of the IEEE Conference on Computer Vision and Pattern Recognition*, 2018, pp. 6848–6856.
- [48] B. Lim, S. Son, H. Kim, S. Nah, and K. M. Lee, "Enhanced deep residual networks for single image super-resolution," *2017 IEEE Conference on Computer Vision and Pattern Recognition Workshops (CVPRW)*, pp. 1132–1140, 2017.
- [49] S. Ioffe and C. Szegedy, "Batch normalization: Accelerating deep network training by reducing internal covariate shift," *ArXiv*, vol. abs/1502.03167, 2015.
- [50] H. Zhao, O. Gallo, I. Frosio, and J. Kautz, "Loss functions for image restoration with neural networks," *IEEE Transactions on Computational Imaging*, vol. 3, no. 1, pp. 47–57, 2017.
- [51] A. Fiszlelew, P. Britos, A. Ochoa, H. Merlino, E. Fernández, and R. García-Martínez, "Finding optimal neural network architecture using genetic algorithms," *Advances in computer science and engineering research in computing science*, vol. 27, pp. 15–24, 2007.
- [52] B. Baker, O. Gupta, R. Raskar, and N. Naik, "Accelerating neural architecture search using performance prediction," *arXiv preprint arXiv:1705.10823*, 2017.
- [53] L. I. Rudin, S. Osher, and E. Fatemi, "Nonlinear total variation based noise removal algorithms," *Physica D Nonlinear Phenomena*, vol. 60, no. 14, pp. 259–268, 1992.
- [54] M. Uecker, F. Ong, J. I. Tamir, D. Bahri, P. Virtue, J. Y. Cheng, T. Zhang, and M. Lustig, "Berkeley advanced reconstruction toolbox," in *Annual Meeting ISMRM, Toronto 2015*, 2015.
- [55] A. Paszke, S. Gross, F. Massa, A. Lerer, J. Bradbury, G. Chanan, T. Killeen, Z. Lin, N. Gimelshein, L. Antiga *et al.*, "Pytorch: An imperative style, high-performance deep learning library," in *Advances in Neural Information Processing Systems*, 2019, pp. 8024–8035.
- [56] D. P. Kingma and J. Ba, "Adam: A method for stochastic optimization," *arXiv preprint arXiv:1412.6980*, 2014.
- [57] R. Caruana, S. Lawrence, and C. L. Giles, "Overfitting in neural nets: Backpropagation, conjugate gradient, and early stopping," in *NIPS*, 2000.
- [58] W. Zhou, B. Alan Conrad, S. Hamid Rahim, and E. P. Simoncelli, "Image quality assessment: from error visibility to structural similarity," *IEEE Trans Image Process*, vol. 13, no. 4, pp. 600–612, 2004.
- [59] C. Peng, X. Zhang, G. Yu, G. Luo, and J. Sun, "Large kernel matters—improve semantic segmentation by global convolutional network," in *Proceedings of the IEEE conference on computer vision and pattern recognition*, 2017, pp. 4353–4361.
- [60] H. Cai, T. Chen, W. Zhang, Y. Yu, and J. Wang, "Efficient architecture search by network transformation," in *Thirty-Second AAAI Conference on Artificial Intelligence*, 2018.